



## Article

# Adsorption Behaviors of Lanthanum (III) and Yttrium (III) Ions on Gibbsite

Zongke Zhou<sup>1</sup>, Quan Wan<sup>1,2</sup> , Wenbin Yu<sup>1</sup> , Xin Nie<sup>1</sup>, Shuguang Yang<sup>1</sup>, Shuqin Yang<sup>1</sup> and Zonghua Qin<sup>1,\*</sup>

<sup>1</sup> State Key Laboratory of Ore Deposit Geochemistry, Institute of Geochemistry, Chinese Academy of Sciences, Guiyang 550051, China; zhouzongke@mail.gyig.ac.cn (Z.Z.); wanquan@vip.gyig.ac.cn (Q.W.); yuwenbin@mail.gyig.ac.cn (W.Y.); niexin@mail.gyig.ac.cn (X.N.); yangshuguang@mail.gyig.ac.cn (S.Y.); yangshuqin@mail.gyig.ac.cn (S.Y.)

<sup>2</sup> CAS Center for Excellence in Comparative Planetology, Hefei 230026, China

\* Correspondence: qinzonghua@mail.gyig.ac.cn

**Abstract:** The enrichment process of rare earth elements in ion-adsorbed rare earth ores and bauxite is potentially related to the adsorption of rare earth elements by gibbsite. In this paper, lanthanum and yttrium were selected as surrogates of light rare earth elements and heavy rare earth elements, respectively. The effects of adsorption time, solution pH, and background electrolyte concentration on the adsorption of rare earth ions by gibbsite were investigated through batch adsorption experiments. The results showed that the adsorption of rare earth ions by gibbsite can approach equilibrium in 72 h. There is mainly electrostatic repulsion between gibbsite and rare earth ions at pH 4–7, and the adsorption efficiency increases with the increase in solution pH value and background electrolyte concentration. The adsorption process of rare earth ions by gibbsite is more consistent with the pseudo-second-order kinetic and Langmuir single-layer adsorption models. Moreover, based on the structural correlation between clay minerals and gibbsite, the causes for the differences in the adsorption behaviors of rare earth elements on the minerals are discussed. The results of this study help to understand the role of aluminum hydroxide in the migration and fate of rare earth elements in epigenetic environments.

**Keywords:** gibbsite; rare earth element; adsorption; kinetics; thermodynamics



**Citation:** Zhou, Z.; Wan, Q.; Yu, W.; Nie, X.; Yang, S.; Yang, S.; Qin, Z.

Adsorption Behaviors of Lanthanum (III) and Yttrium (III) Ions on Gibbsite. *Minerals* **2023**, *13*, 1530.

<https://doi.org/10.3390/min13121530>

Academic Editors: Arjen Van Veelen and Eleanor Spielman-Sun

Received: 17 October 2023

Revised: 25 November 2023

Accepted: 1 December 2023

Published: 9 December 2023



**Copyright:** © 2023 by the authors. Licensee MDPI, Basel, Switzerland. This article is an open access article distributed under the terms and conditions of the Creative Commons Attribution (CC BY) license (<https://creativecommons.org/licenses/by/4.0/>).

## 1. Introduction

Rare earth elements (REE) include 15 lanthanides as well as scandium (Sc) and yttrium (Y). REE are usually divided into light rare earth elements (LREE, also known as the cerium group) and heavy rare earth elements (HREE, also known as the yttrium group). LREE range from lanthanum to europium. HREE range from gadolinium to lutetium, as well as scandium and yttrium. Because of their unique properties, they have a wide range of applications in energy, electronics, aerospace, materials and chemicals, which are listed as critical raw materials by the European Commission [1–3]. The vital role in advanced technology and economic development has led to an increasing demand for rare earth resources. In order to alleviate the supply problem of rare earth resources, it is of great significance to find new alternative sources of rare earth resources on a global scale [4].

As the main source of HREE, ion-adsorbed rare earth ores account for approximately 80% of the world's reserves. They are mainly distributed in southern China [5]. Due to the importance of ion-adsorption-type rare earth ores, the study of the adsorption of rare earth ions on clay minerals has become a hot research area in recent years. Some clay minerals can show good adsorption properties for rare earth ions, such as kaolinite and halloysite [6,7]. Borst et al. found through experimental studies that rare earth ions can be adsorbed on clay minerals such as kaolinite in the form of inner- or outer-sphere complexes [8]. Some studies suggest that the primary adsorption active sites during the adsorption of rare earth ions by clay minerals are on the surface of the aluminum–oxygen octahedral layer [9].

Ishida et al. compared the fluorescence lifetime and intensity of  $\text{Eu}^{3+}$  on kaolinite and gibbsite through time-resolved fluorescence spectroscopy measurements. They found that  $\text{Eu}^{3+}$  can form an inner-sphere complex on the edge surface of the kaolinite's aluminum–oxygen layer under high pH, high background electrolyte concentration, and low  $\text{Eu}^{3+}$  concentration [10]. In addition, by comparing the structures of clay minerals such as kaolinite and montmorillonite with that of gibbsite, it was found that whether 1:1 or 2:1 type clay mineral, its aluminum–oxygen octahedral layer structure is similar to that of gibbsite [11], and this is why the aluminum–oxygen octahedral layer of clay mineral is often called the “gibbsite” layer. Therefore, exploring the adsorption behavior of rare earth ions by gibbsite will help to explain the adsorption mechanism of rare earth ions on clay minerals.

At the same time, REE are also enriched in bauxite, which have been discovered by more and more exploration studies in recent years [12–14]. The REE in some bauxite ores can even reach the industrial mining grade and have colossal resource potential. Specifically, the REE in those bauxite show the characteristics of being more enriched in LREE [15–18]. For example, the aluminum mineral in the bauxite deposit of Yongjiang basin (SW China) is dominated by gibbsite, in which the average content of REE is 763 ppm, with prominent light rare earth enrichment characteristics [19]. The Las Mercedes bauxite deposit in the Dominican Republic mainly comprises gibbsite, clay minerals, and iron minerals, where the REE concentration is generally higher than 1400 ppm [20]. The Samar Island bauxite in the Philippines is mainly composed of gibbsite, boehmite, and iron minerals, with concentrations of REE ranging from 369 ppm to 634 ppm [17]. The aluminum minerals in the bauxite deposits of the Zagros Mountain Belt in Iran are mainly boehmite and gibbsite and a REE content of up to 730 ppm [21]. At present, there have been many speculations on the reason for the enrichment of REE in bauxite. However, the interaction mechanism between aluminum hydroxide minerals and rare earth ions in bauxite is not yet precise. Since the surface of gibbsite is very rich in oxygen and hydroxyl functional groups, studies have confirmed that gibbsite has a specific adsorption capacity for metal ions [22–24], and it is possible that the gibbsite can also adsorb rare earth cations. Therefore, exploring the adsorption of rare earth ions by aluminum hydroxide minerals will help to understand the interaction between aluminum hydroxide minerals and REE in bauxite and then has a guiding significance for explaining the enrichment and differentiation mechanism of REE in bauxite.

In this paper, lanthanum and yttrium as surrogates of LREE and HREE were selected, respectively. Then, a batch experiment method was used to explore the effects of adsorption time, solution pH, background electrolyte concentration, and initial rare earth ion concentration on the adsorption of rare earth ions by gibbsite. Finally, the kinetic and thermodynamic model fitting analyses were proceeded, and a preliminary discussion on the adsorption mechanism was conducted. Based on experimental exploration of the adsorption behavior and mechanism of REE on gibbsite, a preliminary understanding of the role of gibbsite in the enrichment process of REE in bauxite would be obtained.

## 2. Materials and Methods

### 2.1. Characterization of Samples

The phases of the sample were analyzed using a powder X-ray diffractometer with PIXcel<sup>3D</sup> detector (Empyrean, PANalytical, Almelo, The Netherlands). The scanning mode is continuous, scanning range is 4–80° (2 $\theta$ ), the scan speed is 0.22°/s and the total scanning time is approximately 6 min, and Cu-K $\alpha$  ( $\lambda = 0.154$  nm) radiation is used to measure at 40 kV and 40 mA.

The morphology of the samples was observed using a field emission scanning electron microscope (SCIOS, FEI Company, Hillsboro, OR, USA). The accelerating voltage is 2 kV. Before the test, the ethanol dispersion of the sample was dropped onto the monocrystalline silicon wafer, and then dried naturally. Finally, the sample was sprayed with gold.

The sample's point of zero charge was determined using a fully automatic potentiometric titrator (T50, Mettler-Toledo, Greifensee, Switzerland) equipped with a glass

electrode (DGill-SC, Mettler-Toledo). 120 mL of NaNO<sub>3</sub> solution with concentrations of 0.05 and 0.5 mol/L was poured into a 250 mL conical flask containing 3 g of gibbsite. Then, the flask was shaken in a shaker at 25 °C at 200 revolutions per minute (rpm) for 72 h. After shaking, 100 mL of the suspension was added into a titration cup and vented with argon gas until the suspension pH remained unchanged. Subsequently, 0.1 mol/L HNO<sub>3</sub> solution was used to adjust the suspension pH to below 3. After the pH is stable, the suspension was slowly titrated to pH = 11 with 0.1 mol/L NaOH. The intersection of the suspension's titration curves with different background electrolyte concentrations is the point of zero charge (PZC) of the sample.

## 2.2. Adsorption Experiment

The gibbsite sample was purchased from Shanghai Macklin Biochemical Technology Co., Ltd. (Shanghai, China). La(NO<sub>3</sub>)<sub>3</sub>, Y(NO<sub>3</sub>)<sub>3</sub>, and arsenazo III were purchased from Aladdin Scientific Corp. (Cambridge, UK).

For the batch adsorption experiment, a certain amount of La(NO<sub>3</sub>)<sub>3</sub> or Y(NO<sub>3</sub>)<sub>3</sub> solution was poured into a 50 mL stoppered conical flask containing the gibbsite sample. The solid/liquid ratio is 2 g/20 mL, and the initial concentration of rare earth ions is  $3.5 \times 10^{-4}$  mol/L. Use 0.1 mol/L NaOH and HNO<sub>3</sub> to adjust the solution pH. In order to prevent the precipitation of rare earth ions and the dissolution of gibbsite in alkaline solutions, the pH of the solution was selected as 4, 5, 6, and 7 in the experiment. Different amounts of NaNO<sub>3</sub> were added to control the background electrolyte concentration (0.005, 0.050, 0.500 mol/L). The conical flask was sealed and shaken in a shaker at 25 °C and 200 rpm, and then the suspension was filtered through a polyethersulfone (PES) membrane with a pore size of 0.45 μm. The concentrations of rare earth ions in the filtrate were measured using spectrophotometry with arsenazo III [25,26] and calculated by measuring the absorbance at 652 nm with a UV-visible spectrophotometer (UV-vis, Carry 300, Agilent Technologies, Santa Clara, CA, USA). A working curve on the relationship between UV-vis absorbance and REE concentration was measured before each batch of sample testing. For each working curve, R<sup>2</sup> should be greater than 0.995.

When the adsorption time is  $t$ , the adsorption efficiency  $A_t$  (%) for rare earth ions on gibbsite is:

$$A_t = \frac{C_0 - C_t}{C_0} \times 100\% \quad (1)$$

where  $C_0$  is the initial concentration of REE (mol/L);  $C_t$  is the concentration of the unadsorbed REE (mol/L) when the adsorption time is  $t$ . When adsorption reaches equilibrium,  $C_t = C_e$ . When the adsorption time is  $t$ , the adsorption capacity  $Q_t$  (mg/g) is:

$$Q_t = \frac{VM(C_0 - C_t)}{m} \quad (2)$$

where  $V$  is the volume of solution (mL);  $M$  is the molar mass of rare earth ions (g/mol);  $m$  is the mass of gibbsite (g). When adsorption reaches equilibrium,  $Q_t = Q_e$  at  $t = t_e$ .

## 2.3. Adsorption Kinetics

The initial REE concentration was  $3.5 \times 10^{-4}$  mol/L, the initial pH was 7, and the background electrolyte concentration was 0 mol/L. The experimental data within 2 h after the beginning of adsorption were used for the fitting according to pseudo-first-order kinetics and pseudo-second-order kinetics models [27,28]. The nonlinear forms of the pseudo-first-order and pseudo-second-order models are shown in Equations (3) and (4), respectively.

$$Q_t = Q_e \left(1 - e^{-k_1 t}\right) \quad (3)$$

$$Q_t = \frac{k_2 Q_e^2 t}{1 + k_2 Q_e t} \quad (4)$$

where  $Q_t$  and  $Q_e$  (mg/g) are the adsorption capacities of REE by gibbsite at the time  $t$  and equilibrium, respectively.  $k_1$  (1/h) and  $k_2$  (g/(mg·min)) are the adsorption rate constants of pseudo-first-order kinetics and pseudo-second-order kinetics, respectively.

#### 2.4. Adsorption Isotherm and Thermodynamics

The adsorption isotherms of  $\text{La}^{3+}$  and  $\text{Y}^{3+}$  by gibbsite were obtained through batch experiments. The initial rare earth ion concentrations were  $2 \times 10^{-4}$ ,  $3 \times 10^{-4}$ ,  $4 \times 10^{-4}$ ,  $6 \times 10^{-4}$ ,  $8 \times 10^{-4}$ ,  $10 \times 10^{-4}$ ,  $12 \times 10^{-4}$ , and  $14 \times 10^{-4}$  mol/L, respectively. The initial suspension pH is 7; the background electrolyte concentration is 0 mol/L; the adsorption time is 72 h. By calculating the adsorption capacities of REE by gibbsite under different initial rare earth concentrations, the adsorption isotherm was obtained and then fitted using the Langmuir and Freundlich models [29,30].

The Langmuir model describes single-layer adsorption on a uniform surface, and the linear expression is:

$$\frac{C_e}{Q_e} = \frac{1}{KQ_{\max}} + \frac{C_e}{Q_{\max}} \quad (5)$$

where  $C_e$  is the equilibrium concentration of  $\text{La}^{3+}$  or  $\text{Y}^{3+}$ , mg/L;  $Q_e$  is the adsorption capacity, mg/g;  $K$  is the Langmuir constant, L/mg;  $Q_{\max}$  is the maximum adsorption capacity, mg/g.

The Freundlich adsorption isotherm is an empirical formula summarized based on a large amount of experimental data. It is suitable for multi-molecular layer physisorption on non-uniform surfaces. The linear expression is:

$$\lg Q_e = \lg K_F + \frac{1}{n} \lg C_e \quad (6)$$

where  $K_F$  is the Freundlich adsorption coefficient, and  $n$  is a constant.

### 3. Results and Discussions

#### 3.1. Characterization of Gibbsite Samples

The X-ray diffraction pattern of the gibbsite sample is shown in Figure 1. It can be seen from the figure that no other phases except gibbsite are found within the detection range, the characteristic peaks are sharp and narrow, and the sample has good crystallinity. From the scanning electron microscope images of the gibbsite sample (Figure 2), it can be seen that the gibbsite exhibits a typical layered structure. By comparing the morphology of the gibbsite sample before and after the adsorption of REE, it is found that no noticeable changes have occurred in the morphology of the gibbsite.

When the surface charge of a mineral solid is zero, the suspension's pH is the point of zero charge (PZC), and the PZC of an oxide or hydroxide with a uniform surface charge does not change with the background electrolyte concentration [31]. The potentiometric titration curves of the gibbsite under different background electrolyte concentrations (Figure 3) show that the PZC of the gibbsite sample (i.e., the pH at the intersection of the titration curve) is 10.

#### 3.2. Effect of Adsorption Time

Under the conditions of pH 7 and no added background electrolyte, the adsorption efficiency of REE by gibbsite changes with the adsorption time, as shown in Figure 4. The adsorption efficiency surges within the first 2 h and then increases slowly until it approaches equilibrium at 72 h. At 72 h, the adsorption efficiencies of  $\text{La}^{3+}$  and  $\text{Y}^{3+}$  by gibbsite are approximately 70% and 65%, respectively, indicating that the adsorption capacity of gibbsite for LREE is higher than that of HREE. This phenomenon is consistent with the fact that the LREE are more abundant in bauxite [19]. The subsequent adsorption experiments in this study are all conducted for 72 h.

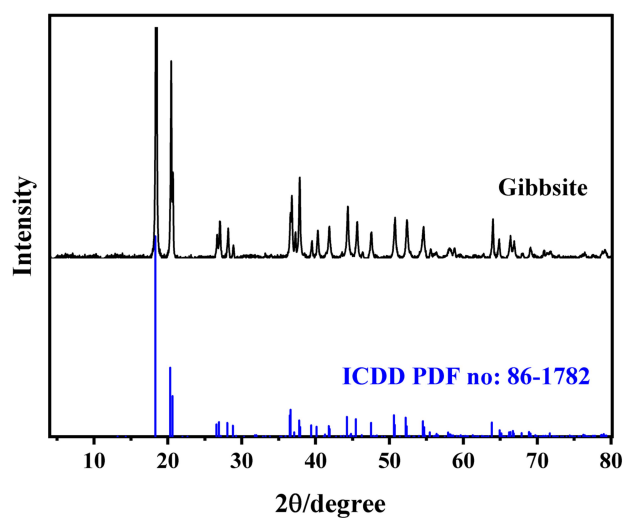


Figure 1. X-ray diffraction pattern of gibbsite sample.

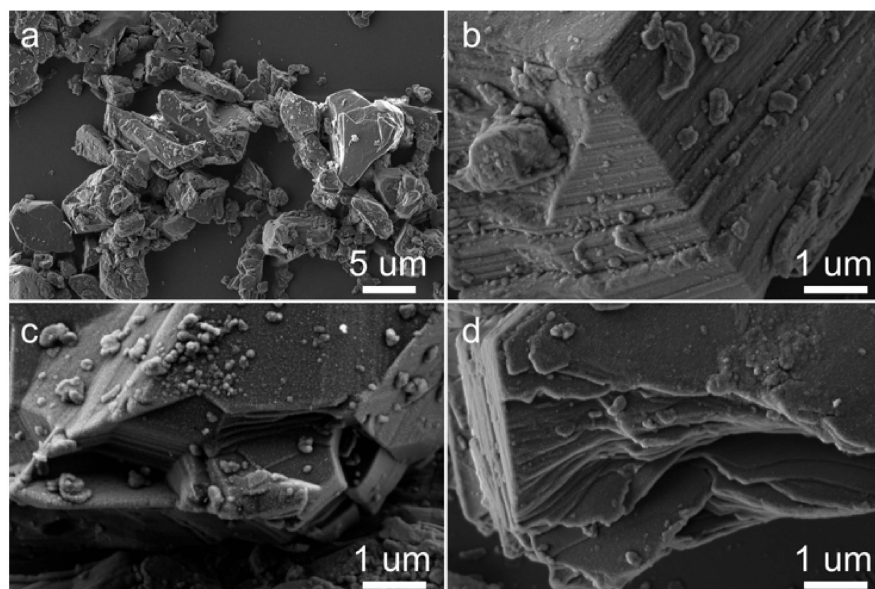


Figure 2. Scanning electron microscope images of gibbsite samples ((a,b) Gibbsite; (c) Gibbsite after the adsorption of  $\text{La}^{3+}$ ; (d) Gibbsite after the adsorption of  $\text{Y}^{3+}$ ).

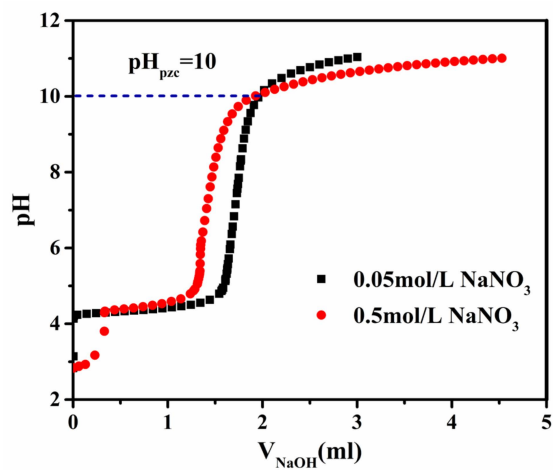


Figure 3. Potentiometric titration curves of gibbsite suspensions under different background electrolyte concentrations.

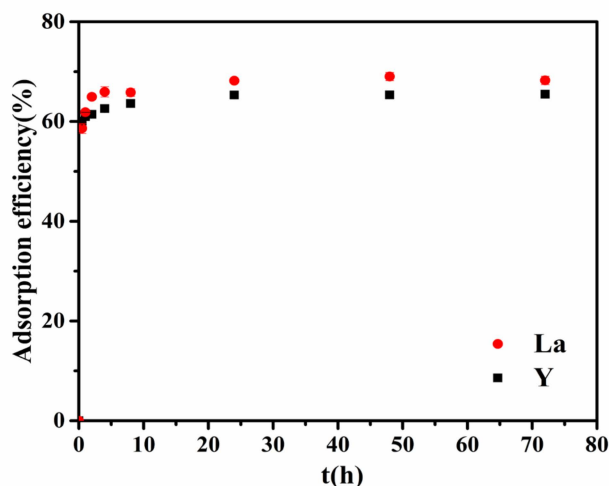


Figure 4. Variations in the adsorption efficiencies of La<sup>3+</sup> and Y<sup>3+</sup> on gibbsite with time.

### 3.3. Effect of pH and Background Electrolyte Concentration

The effects of solution pH and background electrolyte concentration on adsorption are shown in Figure 5. The adsorption behaviors of La<sup>3+</sup> and Y<sup>3+</sup> show similar patterns. Under the same pH conditions, the adsorption efficiency of rare earth cations by gibbsite rises with the increase in background electrolyte concentration; under the same background electrolyte concentration, the adsorption efficiency shows an increasing trend as the pH ascends.

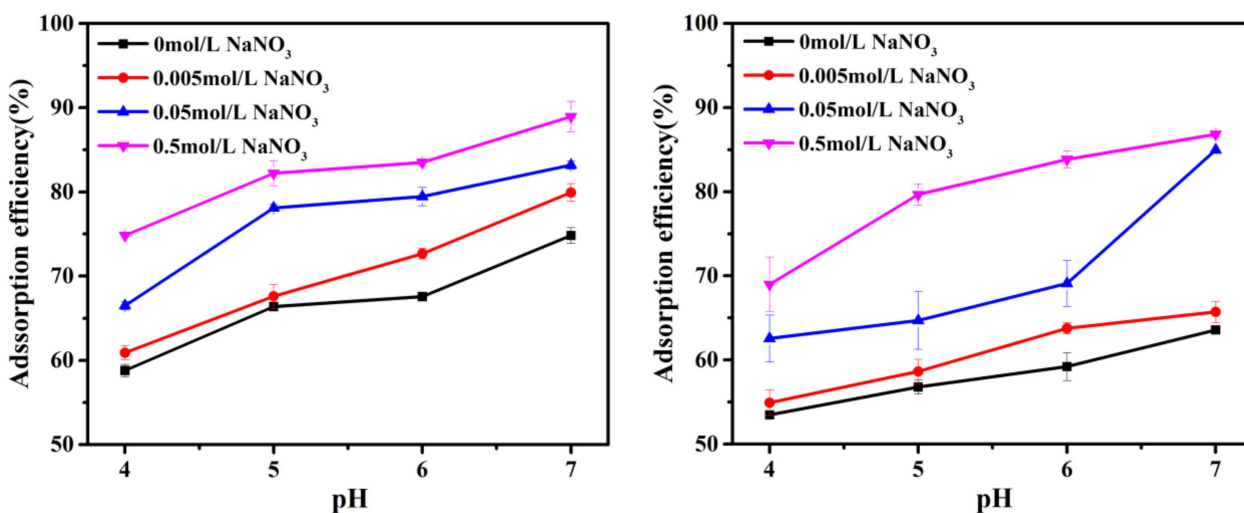


Figure 5. Effects of solution pH and background ion concentration on the adsorption efficiency of La<sup>3+</sup> (left) and Y<sup>3+</sup> (right) on gibbsite.

According to the results of potentiometric titration, the PZC of gibbsite is approximately 10. Therefore, the surface of gibbsite is positively charged due to the protonation effect at pH between 4 and 7. Meanwhile, lanthanum and yttrium mainly exist in the solution in the form of trivalent cations within this pH range. So there is electrostatic repulsion between rare earth cations and gibbsite. As the pH increases, the number of positive charges on the gibbsite surface gradually decreases, and the electrostatic repulsion between the adsorbate and the adsorbent also decreases, which is beneficial to the approach of these cations to the surface. On the other hand, the H<sup>+</sup> concentration decreases with the increasing pH, and the competitive adsorption of hydronium ions with rare earth cations weakens, which is also conducive to the adsorption of rare earth ions by gibbsite. The effect of background electrolyte on adsorption may be attributed to the fact that the increase in

background electrolyte concentration in the solution will compress the electric double layer on the surface of gibbsite, weaken the electrostatic repulsion between gibbsite and rare earth ions, and promote the adsorption between gibbsite and REE. These phenomena are similar to the adsorption behavior of gibbsite to other metal cations [32–34].

### 3.4. Adsorption Kinetics

The adsorption kinetics of  $\text{La}^{3+}$  and  $\text{Y}^{3+}$  by gibbsite were analyzed based on pseudo-first-order and pseudo-second-order models, shown in Figure 6. The kinetic parameters were calculated separately according to the fitting equations, and the results are listed in Table 1. By comparing the correlation coefficients of pseudo-first-order and pseudo-second-order kinetic equations, it was found that the pseudo-second-order kinetic model can better fit the adsorption process of  $\text{La}^{3+}$  and  $\text{Y}^{3+}$  on gibbsite. According to the assumptions of the pseudo-second-order kinetic model, the adsorption rate of rare earth ions by gibbsite is jointly affected by the concentration of rare earth ion and the amount of gibbsite during the adsorption process.

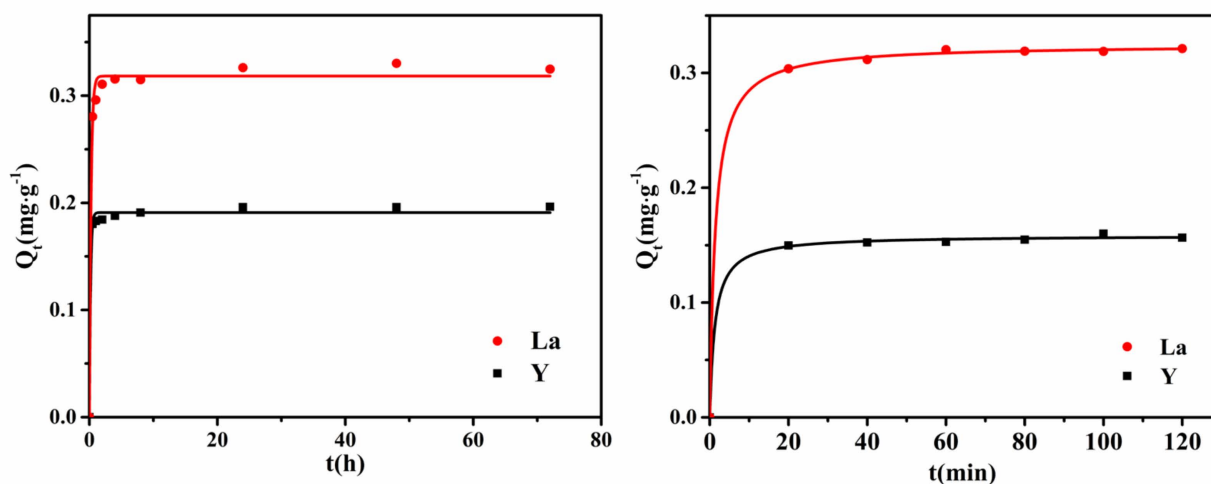


**Figure 6.** Pseudo-first-order (left) and pseudo-second-order (right) kinetic fittings of the adsorption of  $\text{La}^{3+}$  and  $\text{Y}^{3+}$  on gibbsite.

**Table 1.** Fitting parameters of kinetic model for the adsorption of  $\text{La}^{3+}$  and  $\text{Y}^{3+}$  on gibbsite.

Kinetics Model	Pseudo-First-Order Kinetics Model			Pseudo-Second-Order Kinetics Model		
	$Q_e/(\text{mg}\cdot\text{g}^{-1})$	$k_1/(\text{1/h})$	$R^2$	$Q_e/(\text{mg}\cdot\text{g}^{-1})$	$k_2/(\text{g}/\text{mg}\cdot\text{min}^{-1})$	$R^2$
La	0.3183	4.0353	0.9930	0.3247	2.1907	0.9999
Y	0.1909	5.6090	0.9942	0.1584	4.9150	0.9987

### 3.5. Adsorption Isotherms and Thermodynamics

Figure 7 shows the adsorption isotherms of  $\text{La}^{3+}$  and  $\text{Y}^{3+}$  by gibbsite. The equilibrium adsorption capacities of rare earth ions by gibbsite increase sharply at low equilibrium concentrations of REE, and then these isotherms tend to flatten at higher cation concentrations, which suggest the approaching of equilibrium.

The adsorption isotherms are fitted based on the thermodynamic equilibrium model, and the resulting graph is shown in Figure 8. The thermodynamic parameters were calculated based on the linear fitting expressions listed in Table 2. By comparing the correlation coefficients ( $R^2$ ) of the fitting results, it is found that the adsorption processes of  $\text{La}^{3+}$  and  $\text{Y}^{3+}$  on gibbsite are both more consistent with the Langmuir model. Hence, the adsorption process is probably a single-layer adsorption. This is consistent with previous speculations about the formation of inner-sphere complexes between gibbsite and rare earth ions [10]. Therefore, according to the fitting parameters of the Langmuir model,

it can also be seen that the maximum adsorption capacity ( $Q_{max}$ ) of gibbsite for  $La^{3+}$  is approximately 424.9 ppm, and the maximum adsorption capacity ( $Q_{max}$ ) for  $Y^{3+}$  is approximately 261.4 ppm. The adsorption amount of  $La^{3+}$  by gibbsite is more significant than that of  $Y^{3+}$ , probably because  $La^{3+}$  has a larger hydrated ionic radius than  $Y^{3+}$ . Cations in solution usually exist in the form of hydrated ions. For rare earth cations, light rare earth cations are generally nine-coordinated, while heavy rare earth cations tend to be eight-coordinated [8,35,36], making  $La^{3+}$  have a larger hydrated ionic radius than  $Y^{3+}$  radius (2.52 Å for La–O distance and 2.36 Å for Y–O distance) [37]. Therefore, the surface charge density of  $La^{3+}$  is lower than that of  $Y^{3+}$ , and the electrostatic repulsion between  $La^{3+}$  and the mineral surface is weaker than that of  $Y^{3+}$ , which is more conducive to the adsorption of  $La^{3+}$  compared with  $Y^{3+}$ .

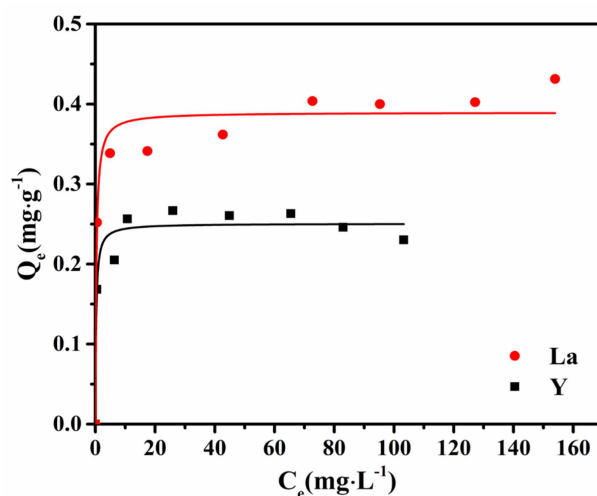


Figure 7. Adsorption isotherms of rare earth cations adsorbed by gibbsite.

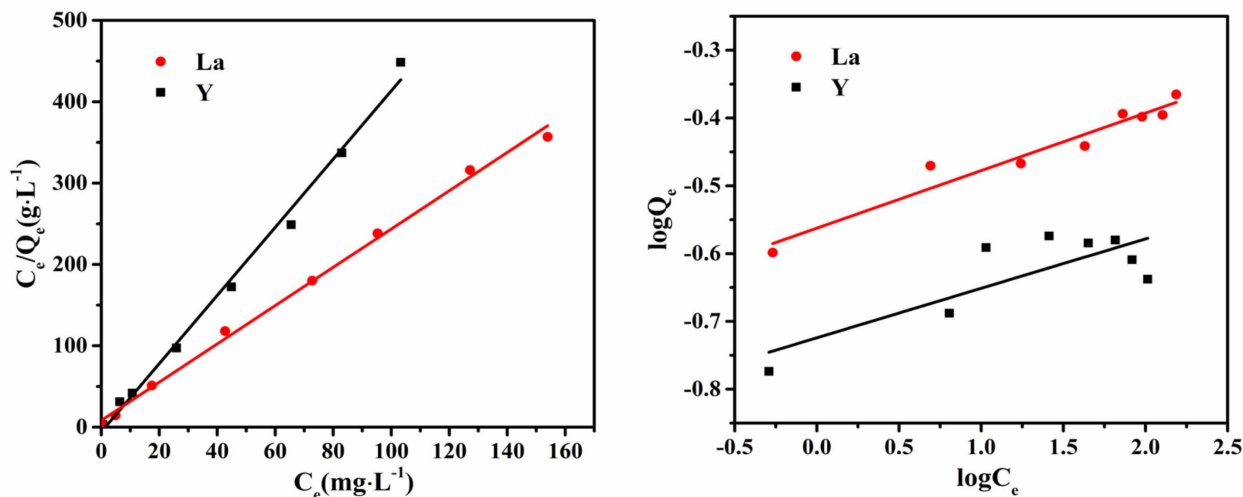


Figure 8. Linear fittings of the adsorption isotherms of  $La^{3+}$  and  $Y^{3+}$  on gibbsite with the Langmuir thermodynamic model (left) and the Freundlich thermodynamic model (right).

### 3.6. Comparison with Adsorption Behavior of Clay Minerals

Clay minerals are usually composed of silicon–oxygen tetrahedral sheets and aluminum–oxygen octahedral sheets. The structure of the aluminum–oxygen octahedral sheets in clay minerals and gibbsite is similar. It is generally considered that the activity of the silanol group is weak ( $SiOH = SiO^- + H^+$ ,  $lgK$  at 25 °C is  $-7.7$  for kaolinite and  $-7.9$  for montmorillonite [9]). However, the enrichment capacities of clay minerals for REE [38] are significantly higher than that of gibbsite.



**Table 2.** Fitting parameters of the thermodynamic models for the adsorption of La<sup>3+</sup> and Y<sup>3+</sup> on gibbsite.

Thermodynamic Model	Langmuir Model			Freundlich Model		
	$Q_{\max}/(\text{mg}\cdot\text{g}^{-1})$	$K/(\text{L}\cdot\text{mg}^{-1})$	$R^2$	$K_F$	$1/n$	$R^2$
La	0.4249	0.0517	0.9964	0.2739	0.0848	0.9456
Y	0.2614	1.0821	0.9936	0.2207	0.0388	0.6537

Take kaolinite as an example, which is a 1:1 type clay mineral and the main occurrence mineral of REE in ion-adsorbed rare earth minerals. Since the isomorphous substitution in the structure is very deficient, it is generally considered to possess little permanent charge, and its active sites for adsorption are mainly surface hydroxyl groups (silanol and aluminol groups). According to our experimental results, the gibbsite's point of zero charge is approximately 10, so the surface of gibbsite is positively charged within the pH range from 4 to 7. From the structure of clay minerals, it can be inferred that the combination of silicon–oxygen sheets makes the structure layers more electronegative. It can be confirmed from the PZCs of kaolinite and montmorillonite (usually <3) [39], which are both higher than gibbsite. This may be one of the reasons for the difference in adsorption behavior of rare earth cations between gibbsite and clay minerals.

On the other hand, other common clay minerals in supergene environments such as montmorillonite and illite have permanently negative charges due to isomorphous substitution in the mineral structure (low-valent cations such as Al<sup>3+</sup> or Mg<sup>2+</sup> replace high-valent cations such as Si<sup>4+</sup> and Al<sup>3+</sup> in the lattice) [40], which can electrostatically attract rare earth cations in a weakly acidic environment and then form surface complexations [41,42]. On the contrary, the gibbsite generally has little permanent negative charge in the layers, and it can be deduced from the adsorption experiment that there is electrostatic repulsion between gibbsite and rare earth ions in a weakly acidic environment. So, the adsorption capacities of REE by clay minerals are significantly more than that of gibbsite. In addition, there are exchangeable interlayer cations in some clay minerals (such as montmorillonite). The interlayer cations can exchange with rare earth ions in the solution during the adsorption process, which is also benefits the adsorption of rare earth ions [43].

It can be seen that unlike gibbsite, the surface of clay minerals is overall negatively charged at weakly acidic pH, and there is electrostatic attraction between it and rare earth cations. Therefore, as the background ion concentration increases, the adsorption capacity decreases; as the pH increases, the protonation effect weakens, and the variable negative charge increases, so the adsorption capacity increases.

#### 4. Conclusions

This paper used batch experiments to explore the adsorption behaviors of REE on gibbsite. The adsorption efficiencies of rare earth ions surge within the first 2 h, then increase slowly until close to equilibrium at 72 h. According to the results of potentiometric titration experiments, the interaction between gibbsite and rare earth ions is mainly electrostatic repulsion within the pH range of this study, and the adsorption capacity of rare earth ions rises with the increase in pH and background electrolyte concentration in the solution. These may suggest that rare earth ions may form an inner-sphere complex with the surface aluminols of gibbsite. Through model fitting of the kinetics and thermodynamics of the adsorption process, it was found that the adsorption process of rare earth ions by gibbsite is more consistent with the pseudo-second-order kinetic model and the Langmuir single-layer adsorption model. The adsorption capacity of light rare earths by gibbsite is higher than that of heavy rare earths, possibly because light REE have larger hydrated ionic radii. This phenomenon is consistent with the fact that LREE are more enriched than HREE in bauxite. Therefore, based on the experimental results, gibbsite may contribute to the enrichment and differentiation process of REE in bauxite. Moreover, clay minerals are generally more negatively charged, resulting from the combination of silicon–oxygen

sheets and the isomorphic substitution in the layers compared with gibbsite, which causes the high capacity of REE adsorbed on clay minerals. The results of this study would help to understand the role of aluminum hydroxide in the migration and fate of REE in epigenetic environments.

**Author Contributions:** Conceptualization, Z.Q., W.Y., X.N. and Q.W.; methodology, Z.Q. and Z.Z.; investigation, Z.Q. and Z.Z.; resources, Z.Q. and Q.W.; funding acquisition, Z.Q. and Q.W.; data curation, Z.Q. and Z.Z.; project administration, S.Y. (Shuguang Yang) and S.Y. (Shuqin Yang); writing—original draft preparation, Z.Q. and Z.Z.; writing—review and editing, Z.Q. and Q.W.; visualization, Z.Q.; supervision, Z.Q. and Q.W. All authors have read and agreed to the published version of the manuscript.

**Funding:** This work was financially supported by the National Natural Science Foundation of China (41872046), the B-type Strategic Priority Program of the Chinese Academy of Sciences (XDB41000000), the Guizhou Provincial Basic Research Program (Natural Science): [2019]1460, and the Frontier Program of State Key Laboratory of Ore Deposit Geochemistry (SKLOGD-2018-01).

**Data Availability Statement:** Data will be made available on request.

**Conflicts of Interest:** The authors declare no conflict of interest.

## References

1. Patel, K.S.; Sharma, S.; Maity, J.P.; Martin-Ramos, P.; Fiket, Z.; Bhattacharya, P.; Zhu, Y.B. Occurrence of uranium, thorium and rare earth elements in the environment: A review. *Front. Environ. Sci.* **2023**, *10*, 1058053. [[CrossRef](#)]
2. Balaram, V. Potential Future Alternative Resources for Rare Earth Elements: Opportunities and Challenges. *Minerals* **2023**, *13*, 425. [[CrossRef](#)]
3. Swain, B. Red mud: An environmental challenge but overlooked treasure for critical rare earth metals. *MRS Bull.* **2022**, *47*, 289–302. [[CrossRef](#)]
4. Dushyantha, N.; Ratnayake, N.; Premasiri, R.; Batapola, N.; Panagoda, H.; Jayawardena, C.; Chandrajith, R.; Ilankoon, I.; Rohitha, S.; Ratnayake, A.S.; et al. Geochemical exploration for prospecting new rare earth elements (REEs) sources: REE potential in lake sediments around Eppawala Phosphate Deposit, Sri Lanka. *J. Asian Earth Sci.* **2023**, *243*, 105515. [[CrossRef](#)]
5. Mancheri, N.A.; Sprecher, B.; Bailey, G.; Ge, J.; Tukker, A. Effect of Chinese policies on rare earth supply chain resilience. *Resour. Conserv. Recycl.* **2019**, *142*, 101–112. [[CrossRef](#)]
6. Yang, M.J.; Liang, X.L.; Ma, L.Y.; Huang, J.; He, H.P.; Zhu, J.X. Adsorption of REEs on kaolinite and halloysite: A link to the REE distribution on clays in the weathering crust of granite. *Chem. Geol.* **2019**, *525*, 210–217. [[CrossRef](#)]
7. Alshameri, A.; He, H.; Xin, C.; Zhu, J.; Xinghu, W.; Zhu, R.; Wang, H. Understanding the role of natural clay minerals as effective adsorbents and alternative source of rare earth elements: Adsorption operative parameters. *Hydrometallurgy* **2019**, *185*, 149–161. [[CrossRef](#)]
8. Borst, A.M.; Smith, M.P.; Finch, A.A.; Estrade, G.; Villanova-de-Benavent, C.; Nason, P.; Marquis, E.; Horsburgh, N.J.; Goodenough, K.M.; Xu, C.; et al. Adsorption of rare earth elements in regolith-hosted clay deposits. *Nat. Commun.* **2020**, *11*, 4386. [[CrossRef](#)]
9. Tertre, E.; Berger, G.; Simoni, E.; Castet, S.; Giffaut, E.; Loubet, M.; Catalette, H. Europium retention onto clay minerals from 25 to 150 °C: Experimental measurements, spectroscopic features and sorption modelling. *Geochim. Cosmochim. Acta* **2006**, *70*, 4563–4578. [[CrossRef](#)]
10. Ishida, K.; Saito, T.; Aoyagi, N.; Kimura, T.; Nagaishi, R.; Nagasaki, S.; Tanaka, S. Surface speciation of Eu<sup>3+</sup> adsorbed on kaolinite by time-resolved laser fluorescence spectroscopy (TRLFS) and parallel factor analysis (PARAFAC). *J. Colloid Interface Sci.* **2012**, *374*, 258–266. [[CrossRef](#)]
11. Brigatti, M.F.; Galán, E.; Theng, B.K.G. Structure and mineralogy of clay minerals. In *Handbook of Clay Science*, 2nd ed.; Bergaya, F., Lagaly, G., Eds.; Developments in Clay Science; Elsevier: Amsterdam, The Netherlands, 2013; pp. 21–81.
12. Abedini, A.; Mongelli, G.; Khosravi, M.; Sinisi, R. Geochemistry and secular trends in the middle-late Permian karst bauxite deposits, northwestern Iran. *Ore Geol. Rev.* **2020**, *124*, 103660. [[CrossRef](#)]
13. Mondillo, N.; Di Nuzzo, M.; Kalaitzidis, S.; Boni, M.; Santoro, L.; Balassone, G. Petrographic and geochemical features of the B3 bauxite horizon (Cenomanian-Turonian) in the Parnassos-Ghiona area: A contribution towards the genesis of the Greek karst bauxites. *Ore Geol. Rev.* **2022**, *143*, 104759. [[CrossRef](#)]
14. Abedini, A.; Khosravi, M. REE Geochemical Characteristics of the Huri Karst-Type Bauxite Deposit, Irano-Himalayan Belt, Northwestern Iran. *Minerals* **2023**, *13*, 926. [[CrossRef](#)]
15. Gamaletsos, P.N.; Godelitsas, A.; Filippidis, A.; Pontikes, Y. The Rare Earth Elements Potential of Greek Bauxite Active Mines in the Light of a Sustainable REE Demand. *J. Sustain. Metall.* **2019**, *5*, 20–47. [[CrossRef](#)]

16. Deady, E.A.; Mouchos, E.; Goodenough, K.; Williamson, B.J.; Wall, F. A review of the potential for rare-earth element resources from European red muds: Examples from Seydisheir, Turkey and Parnassus-Giona, Greece. *Mineral. Mag.* **2016**, *80*, 43–61. [[CrossRef](#)]
17. Gibaga, C.R.L.; Samaniego, J.O.; Tanciongco, A.M.; Quierrez, R.N.M.; Montano, M.O.; Gervasio, J.H.C.; Reyes, R.C.G.; Peralta, M.J.V. The rare earth element (REE) potential of the Philippines. *J. Geochem. Explor.* **2022**, *242*, 107082. [[CrossRef](#)]
18. Long, K.; Fu, Y.; Long, Z.; Tian, J.; Zheng, J. Resource potential analysis of REE and Sc in global bauxite. *Acta Geol. Sin.* **2019**, *93*, 1279–1295.
19. Chen, J.; Wang, Q.; Zhang, Q.; Carranza, E.J.M.; Wang, J. Mineralogical and geochemical investigations on the iron-rich gibbsitic bauxite in Yongjiang basin, SW China. *J. Geochem. Explor.* **2018**, *188*, 413–426. [[CrossRef](#)]
20. Torró, L.; Proenza, J.A.; Aiglsperger, T.; Bover-Arnal, T.; Villanova-de-Benavent, C.; Rodríguez-García, D.; Ramírez, A.; Rodríguez, J.; Mosquea, L.A.; Salas, R. Geological, geochemical and mineralogical characteristics of REE-bearing Las Mercedes bauxite deposit, Dominican Republic. *Ore Geol. Rev.* **2017**, *89*, 114–131. [[CrossRef](#)]
21. Zarasvandi, A.; Charchi, A.; Carranza, E.J.M.; Alizadeh, B. Karst bauxite deposits in the Zagros Mountain Belt, Iran. *Ore Geol. Rev.* **2008**, *34*, 521–532. [[CrossRef](#)]
22. Baumer, T.; Kay, P.; Hixon, A.E. Comparison of europium and neptunium adsorption to aluminum (hydr)oxide minerals. *Chem. Geol.* **2017**, *464*, 84–90. [[CrossRef](#)]
23. Tokoro, C.; Sakakibara, T.; Suzuki, S. Mechanism investigation and surface complexation modeling of zinc sorption on aluminum hydroxide in adsorption/coprecipitation processes. *Chem. Eng. J.* **2015**, *279*, 86–92. [[CrossRef](#)]
24. Ogata, F.; Tominaga, H.; Yabutani, H.; Taga, A.; Kawasaki, N. Granulation of gibbsite with inorganic binder and its ability to adsorb Mo(VI) from aqueous solution. *Toxicol. Environ. Chem.* **2012**, *94*, 650–659. [[CrossRef](#)]
25. Guo, X.M.; Yan, Q.C.; Meng, X.T.; Ma, R.X. UV-Visible Spectrophotometry with Arsenazo III for the Determination of Samarium. *J. Appl. Spectrosc.* **2019**, *86*, 542–548. [[CrossRef](#)]
26. Savvin, S.B. Analytical use of arsenazo III: Determination of thorium, zirconium, uranium and rare earth elements. *Talanta* **1961**, *8*, 673–685. [[CrossRef](#)]
27. Revellame, E.D.; Fortela, D.L.; Sharp, W.; Hernandez, R.; Zappi, M.E. Adsorption kinetic modeling using pseudo-first order and pseudo-second order rate laws: A review. *Clean. Eng. Technol.* **2020**, *1*, 100032. [[CrossRef](#)]
28. Sen Gupta, S.; Bhattacharyya, K.G. Kinetics of adsorption of metal ions on inorganic materials: A review. *Adv. Colloid Interface Sci.* **2011**, *162*, 39–58. [[CrossRef](#)]
29. Al-Ghouti, M.A.; Da'ana, D.A. Guidelines for the use and interpretation of adsorption isotherm models: A review. *J. Hazard. Mater.* **2020**, *393*, 122383. [[CrossRef](#)]
30. Foo, K.Y.; Hameed, B.H. Insights into the modeling of adsorption isotherm systems. *Chem. Eng. J.* **2010**, *156*, 2–10. [[CrossRef](#)]
31. Pechenyuk, S.I. The use of the pH at the point of zero charge for characterizing the properties of oxide hydroxides. *Russ. Chem. Bull.* **1999**, *48*, 1017–1023. [[CrossRef](#)]
32. Tochiyama, O.; Yamazaki, H.; Li, N. Effect of the concentration of metal ions on their adsorption on various hydrous iron and aluminum oxides. *J. Nucl. Sci. Technol.* **1996**, *33*, 846–851. [[CrossRef](#)]
33. Ahmed, A.; Yujun, W.; Johannes, L.; Marcelo Eduardo, A. Calcium Uptake on Kaolinite and Gibbsite: Effects of Sulfate, pH, and Salt Concentration with Additional Insight from Second Harmonic Generation on Temperature Dependencies with Sapphire-Basal Planes and the Potential Relevance to Ice Nucleation. In *Advanced Sorption Process Applications*; Serpil, E., Ed.; IntechOpen: Rijeka, Croatia, 2018; pp. 1–22.
34. Saeki, K. Adsorption of Fe<sup>2+</sup> and Mn<sup>2+</sup> on silica, gibbsite, and humic acids. *Soil Sci.* **2004**, *169*, 832–840. [[CrossRef](#)]
35. Persson, I.; D'Angelo, P.; De Panfilis, S.; Sandström, M.; Eriksson, L. Hydration of Lanthanoid(III) Ions in Aqueous Solution and Crystalline Hydrates Studied by EXAFS Spectroscopy and Crystallography: The Myth of the “Gadolinium Break”. *Chem. Eur. J.* **2008**, *14*, 3056–3066. [[CrossRef](#)] [[PubMed](#)]
36. Peters, J.A.; Djanashvili, K.; Gerald, C.F.G.C.; Platas-Iglesias, C. The chemical consequences of the gradual decrease of the ionic radius along the Ln-series. *Coord. Chem. Rev.* **2020**, *406*, 213146. [[CrossRef](#)]
37. Persson, I. Hydrated metal ions in aqueous solution: How regular are their structures? *Pure Appl. Chem.* **2010**, *82*, 1901–1917. [[CrossRef](#)]
38. Coppin, F.; Berger, G.; Bauer, A.; Castet, S.; Loubet, M. Sorption of lanthanides on smectite and kaolinite. *Chem. Geol.* **2002**, *182*, 57–68. [[CrossRef](#)]
39. Kosmulski, M. The pH dependent surface charging and points of zero charge. X. Update. *Adv. Colloid Interface Sci.* **2023**, *319*, 102973. [[CrossRef](#)]
40. Hirst, C.; Andersson, P.S.; Shaw, S.; Burke, I.T.; Kutscher, L.; Murphy, M.J.; Maximov, T.; Pokrovsky, O.S.; Morth, C.-M.; Porcelli, D. Characterisation of Fe-bearing particles and colloids in the Lena River basin, NE Russia. *Geochim. Cosmochim. Acta* **2017**, *213*, 553–573. [[CrossRef](#)]
41. Wainippee, W.; Cuadros, J.; Sephton, M.A.; Unsworth, C.; Gill, M.G.; Strelkopytov, S.; Weiss, D.J. The effects of oil on As(V) adsorption on illite, kaolinite, montmorillonite and chlorite. *Geochim. Cosmochim. Acta* **2013**, *121*, 487–502. [[CrossRef](#)]

42. Yusoff, Z.M.; Ngwenya, B.T.; Parsons, I. Mobility and fractionation of REEs during deep weathering of geochemically contrasting granites in a tropical setting, Malaysia. *Chem. Geol.* **2013**, *349*, 71–86. [[CrossRef](#)]
43. Granados-Correa, F.; Vilchis-Granados, J.; Jimenez-Reyes, M.; Quiroz-Granados, L.A. Adsorption Behaviour of La(III) and Eu(III) Ions from Aqueous Solutions by Hydroxyapatite: Kinetic, Isotherm, and Thermodynamic Studies. *J. Chem.* **2013**, *2013*, 751696. [[CrossRef](#)]

**Disclaimer/Publisher's Note:** The statements, opinions and data contained in all publications are solely those of the individual author(s) and contributor(s) and not of MDPI and/or the editor(s). MDPI and/or the editor(s) disclaim responsibility for any injury to people or property resulting from any ideas, methods, instructions or products referred to in the content.